CONF-960202--24

LA-UR-~~95~~ 96-0602

Title:

MECHANICAL PROPERTIES AND CONSTITUTIVE RELATIONS FOR TANTALUM AND TANTALUM ALLOYS UNDER HIGH-RATE DEFORMATION

RECEIVED
APR 12 1996
OSTI

Author(s): **S. R. Chen, G. T. Gray III, S. R. Bingert**

Materials Science and Technology Division
Los Alamos National Laboratory
Los Alamos, NM 87545

Submitted to:

TANTALUM
1996 ANNUAL MEETING
February 4-8, 1996

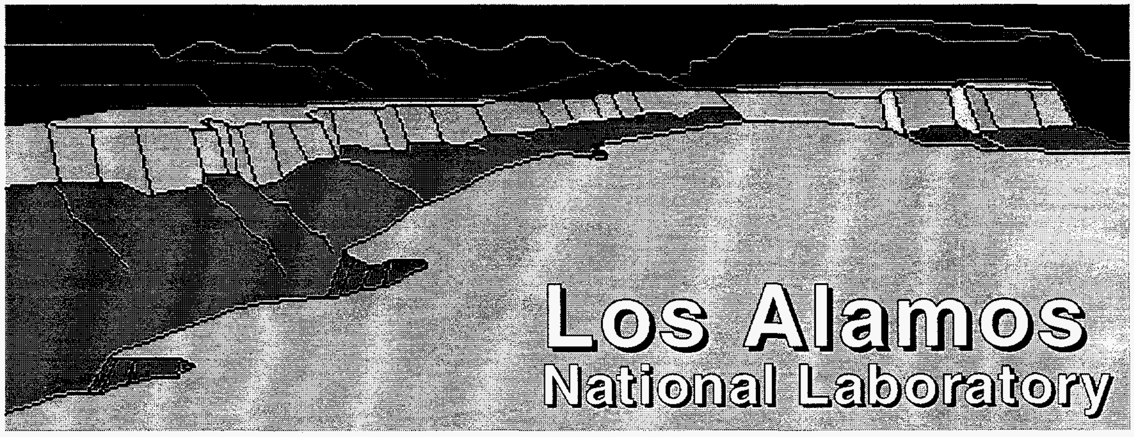

Los Alamos National Laboratory, an affirmative action/equal opportunity employer, is operated by the University of California for the U.S. Department of Energy under contract W-7405-ENG-36. By acceptance of this article, the publisher recognizes that the U.S. Government retains a nonexclusive, royalty-free license to publish or reproduce the published form of this contribution, or to allow others to do so, for U.S. Government purposes. The Los Alamos National Laboratory requests that the publisher identify this article as work performed under the auspices of the U.S. Department of Energy.
This is a preprint of a paper intended for publication in a journal or proceedings. Because changes may be made before publication, this preprint is made available with the understanding that it will not be cited or reproduced without the permission of the author.

MASTER

DISTRIBUTION OF THIS DOCUMENT IS UNLIMITED

DISCLAIMER

Portions of this document may be illegible in electronic image products. Images are produced from the best available original document.

MECHANICAL PROPERTIES AND CONSTITUTIVE RELATIONS FOR TANTALUM AND TANTALUM ALLOYS UNDER HIGH-RATE DEFORMATION

S.R. Chen, G.T. Gray III, and S.R. Bingert

Materials Science and Technology Division
Los Alamos National Laboratory
Los Alamos, New Mexico 87545

Abstract

Tantalum and its alloys have received increased interest as a model bcc metal and for defense-related applications. The stress-strain behavior of several tantalums, possessing varied compositions and manufacturing histories, and tantalum alloyed with tungsten, was investigated as a function of temperature from -196°C to 1000°C, and strain rate from 10^{-3} s^{-1} to 8000 s^{-1}. The yield stress for all the Ta-materials was found to be sensitive to the test temperature, the impurity and solute contents; however, the strain hardening remained very similar for various "pure" tantalums but increased with alloying. Powder-metallurgy (P/M) tantalum with various levels of oxygen content produced via different processing paths was also investigated. Similar mechanical properties compared to conventionally processed tantalums were achieved in the P/M Ta. This data suggests that the frequently observed inhomogeneities in the mechanical behavior of tantalum inherited from conventional processes can be overcome. Constitutive relations based upon the Johnson-Cook, the Zerilli-Armstrong, and the Mechanical Threshold Stress models were evaluated for all the Ta-based materials. Parameters were also fit for these models to a tantalum-bar material. Flow stresses of a Ta bar stock subjected to a large-strain deformation of ε=1.85 via multiple upset forging were obtained. The capabilities and limitations of each model for large-strain applications are examined. The deformation mechanisms controlling high-rate plasticity in tantalum are revisited.

Introduction

The microstructure / property relationships of tantalum and tantalum-based alloys continue to attract scientific and engineering interest due to their high density, melting point, excellent formability, good heat conductivity, good fracture toughness (even at low temperatures), corrosion resistance, and their weldability[1]. Since 1950 numerous studies have probed the microstructure-chemistry/property response of a large number of tantalum and tantalum-based alloys, both in single-crystal and polycrystalline form[1-5]. Tantalum, like all bcc metals exhibits deformation behavior which is markedly influenced by impurities, alloying additions, crystallographic texture, temperature, and strain rate[2-8]. Tantalum and its alloys are increasingly being utilized in defense-related applications where their mechanical properties under high-strain-rate deformation have proven desirable. In this paper a wide range of data on unalloyed wrought tantalum, powder-metallurgy tantalum, and Ta-W alloys subjected to high-strain-rate compression at various temperatures will be presented. The yield and flow stresses for all the Ta-based materials are shown to be sensitive to changes in temperature and strain rate at low temperatures and/or high strain rates. A large Peierls stress in bcc materials has been proposed as the rate-controlling mechanism in this temperature and strain-rate regime[7,9]. This large intrinsic lattice resistance results in restricted movement of screw dislocations; long straight screw segments are often observed in this class of materials after deformation[3,7,10]. This suppression of cross-slip of screw dislocations results in linear glide and therefore lower overall strain-hardening rates[11]. Strain hardening rates in this class of materials under low temperature or high strain rates loading states are also seen to be temperature insensitive and to first order strain independent[2,7]. The addition of alloying solutes to tantalum raises the yield and flow stresses through solid solution strengthening[7]. The overall work-hardening rate is increased relative to un-alloyed Ta due to dislocation-solute interactions. While a large number of studies have probed the mechanical behavior of a broad spectrum of tantalum alloys the details of the underlying deformation mechanisms remain poorly understood and in some cases controversial[3,7,9,12].

The widespread utilization of modern high-speed computers makes it possible to develop more sophisticated material constitutive model descriptions capable of modeling complex problems[13-15]. An accurate description of a materials response over a wide range of loading environments, as well as having predictive capabilities outside the measured range, is in great demand. The material properties unique to bcc metals and alloys bring many challenges to the development of physically-based constitutive models. The influence of impurities and the effect of tungsten alloying on the constitutive behavior of Ta and Ta-W alloys will be presented in this paper. Several currently utilized constitutive models, namely the Mechanical Threshold Stress model[16], the Johnson-Cook model[17], and the Zerilli-Armstrong model[18], were examined. The same data set is used to derive the parameters for each model enabling direct comparisons between each model.

Experimental

Materials

Several commercially-pure tantalums and tantalum-tungsten alloys in both plate and bar form were used in this study. The compositions and the designation for each material are listed in Table I. Most of the materials studied were purchased from Cabot Corporation. The materials were all tested in a well annealed condition. Detailed characterization of a Ta-bar material as to the effects of annealing temperature, texture, microstructure, and large-strain deformation are presented in this volume. Several batches of small quantities of tantalum were produced via power metallurgy at LANL (designated Ta-48A and Ta-48B in Table I). Processing procedures and the influence of some important variables such as impurity contents, temperatures and pressure are outlined elsewhere in this proceedings. The mechanical properties of the P/M materials will be addressed in this paper.

Table I Alloy Compositions (in weight ppm)

	Form	C	O	N	H	W	Nb
Ta-DD	plate	12	<50	<10	<5	60	250
Ta-bar	bar	10	65	20	<5	<25	80
Ta-A	plate	9	44	18	<1	<150	123
Ta-48A*	P/M	<10	841	61	22	N/A	N/A
Ta-48B*	P/M	<10	234	35	651	N/A	N/A
Ta-2.5W	plate	18	98	<10	<5	24,000	330
Ta-5W	plate	15	<50	<10	<5	52,000	65
Ta-10W	plate	11	63	<10	<5	96,200	385

*composition of the as-received powders.

The mechanical responses of the tantalum materials were measured in compression using solid-cylindrical samples nominally 6-mm in diameter by 6-mm long, lubricated with molybdenum grease. An initial description of the influence of tungsten alloying on the mechanical properties and texture of Ta was published previously.[19] Quasi-static compression tests were conducted at strain rates of 10^{-3} and 10^{-1} s^{-1} at -196°C and 25°C. Dynamic tests, strain rates of 1000-8000 s^{-1}, were conducted from -196°C to 1000°C in vacuum utilizing a Split-Hopkinson Pressure Bar.[20] The inherent oscillations in the dynamic stress-strain curves and the lack of stress equilibrium in the specimens at low strains make the determination of yield inaccurate at high strain rates.

Description of Models

The constitutive equations used in this study are as follows:

Johnson-Cook Model (JC):[17]

$$\sigma = (A + B\cdot\varepsilon_p{}^n)(1 + C\cdot\ln\dot{\varepsilon}^*)(1 - T^{*m}) \tag{1}$$

where $\dot{\varepsilon}^*$ is a non-dimensional strain rate value, ε_p is the plastic strain, and T^* is $(T - T_{Room})/(T_{Melt} - T_{Room})$.

Zerilli-Armstrong Model (ZA) for body-centered cubic material:[18]

$$\sigma = C_0 + C_1\cdot\exp(-C_3\cdot T + C_4\cdot T\cdot\ln\dot{\varepsilon}) + C_5\cdot\varepsilon_p{}^n \tag{2}$$

The athermal stress term C_0 can be modified to include grain size effects using a Hall-Petch relation $\sigma_0 + k\cdot d^{-1/2}$, where d is the average grain size. In the ZA model, it is presumed that the work hardening rate is independent of temperature and strain rate. Both the JC and ZA models use a power-law stress-strain relationship that exhibits continual work hardening without approaching a saturation stress at large strains; i.e., both models predict infinite stresses at infinite strains.

Mechanical Threshold Stress Model (MTS):

The fundamental dislocation kinetics theories underpinning this model and detailed description of the mechanical threshold stress (MTS) model have been presented in detail previously[16,21-23]. A brief summary of the equations used in the MTS model is presented here. Plastic deformation is known to be controlled by the thermally-activated interactions of dislocations with obstacles. In the MTS model the current structure at any point during the deformation process is represented by an internal state variable, the mechanical threshold which is defined as the flow stress at 0K. This mechanical threshold stress is separated into athermal and thermal components. The athermal component characterizes the rate independent interactions of dislocations with long-range barriers such as grain boundaries or second-phase particles or dispersoids, such as in composites. The thermal component characterizes the rate dependent interactions of dislocations with short range obstacles (forest dislocations, interstitial, solutes, Peierls barrier, etc.) that can be overcome with the assistance of thermal activation. The stress of a constant structure at a given deformation condition can be expressed in terms of the mechanical threshold as

$$\frac{\sigma}{\mu} = \frac{\sigma_a}{\mu} + \sum S(\dot{\varepsilon},T)\frac{\hat{\sigma}_t}{\mu_0}, \tag{3}$$

where the athermal component is a function of temperature only through the shear modulus (μ), and the factor S specifies the ratio between the applied stress and the mechanical threshold stress. This factor is smaller than 1 for thermally activated controlled glide because of the contribution of thermal activation. The form for S is written as[11]:

$$S = \left[1 - \left(\frac{kT}{g_0\mu b^3}\ln\frac{\dot{\varepsilon}_0}{\dot{\varepsilon}}\right)^{1/q}\right]^{1/p}. \tag{4}$$

For single phase materials with cubic crystal structures, the thermal component consists of the linear summation of a term describing the yield stress and a term describing the evolution of the dislocation structure as a function of temperature, strain rate and strain. Equation (3) can be written as

$$\frac{\sigma}{\mu} = \frac{\sigma_a}{\mu} + S_i(\dot{\varepsilon},T)\frac{\hat{\sigma}_i}{\mu_0} + S_\varepsilon(\dot{\varepsilon},T)\frac{\hat{\sigma}_\varepsilon}{\mu_0}. \tag{5}$$

The second term on the right hand side of the equation describes the rate dependence of the yield stress mainly due to intrinsic barriers such as the strong Peierls stress observed in bcc materials at low temperatures or at high strain rates. It is further assumed that this term doesn't evolve after yielding. $\hat{\sigma}_\varepsilon$ in equation (5) evolves with strain due to dislocation accumulation (work hardening) and annihilation (recovery). The physical understanding of the work hardening behavior of polycrystals is still inadequate to unify this complex process and represent it by physically-based parameters. Follansbee et al.[16] have chosen the following form to fit the work hardening to their experimental data:

$$\theta = \theta_0 \left\{ 1 - \frac{\tanh\left[\alpha \dfrac{\hat{\sigma}_\varepsilon}{\hat{\sigma}_{\varepsilon s}(\dot{\varepsilon},T)}\right]}{\tanh(\alpha)} \right\}, \tag{6}$$

where α approaches zero represents a linear variation of strain hardening rate with stress (Voce law). The saturation threshold stress $\hat{\sigma}_{\varepsilon s}$ is a function of temperature and strain rate according to:[24-26]

$$\hat{\sigma}_{\varepsilon s} = \hat{\sigma}_{\varepsilon s0}\left(\frac{\dot{\varepsilon}}{\dot{\varepsilon}_{\varepsilon s0}}\right)^{1/n}, \tag{7}$$

where $n = g_{0\varepsilon s}\mu b^3/kT$, $\dot{\varepsilon}_{\varepsilon s0}$, $g_{0\varepsilon s}$, and $\hat{\sigma}_{\varepsilon s0}$ are constants.

The shear modulus was calculated for body-centered cubic (bcc) Ta using the formula:

$$\mu = \frac{(C_{11} - C_{12} + C_{44})}{3} \tag{8}$$

where C_{ij} are the elastic constants[27]. For simplicity, an empirical equation[28] was used to fit the data to incorporate the temperature dependence of "μ" in a form of

$$\mu = \mu_0 - \frac{D}{\exp\left(\dfrac{T_0}{T}\right) - 1}. \tag{9}$$

The temperature rise for the tests at strain rates above 500 s^{-1} can be calculated assuming a certain percentage (Ψ) of the work of plastic deformation is converted into heat according to:

$$\Delta T = \frac{\Psi}{\rho C_p}\int \sigma(\varepsilon)d\varepsilon \tag{10}$$

where σ and ε are the true stress and strain, ρ is the density, and C_p is the heat capacity that can be written in the form[29] of

$$A_0 + A_1 \cdot T + A_2 / T^2. \tag{11}$$

Adiabatic heating is expected to make a large difference at higher strains during high-rate deformation.

Results and Discussions

Mechanical Responses

The effect of temperature and strain rate on the mechanical properties of the Ta-materials was investigated through a series of compression tests over wide range of temperatures and strain rates. The compressive stress-strain responses of the different Ta and Ta-W alloys are shown in Figures 1-5.

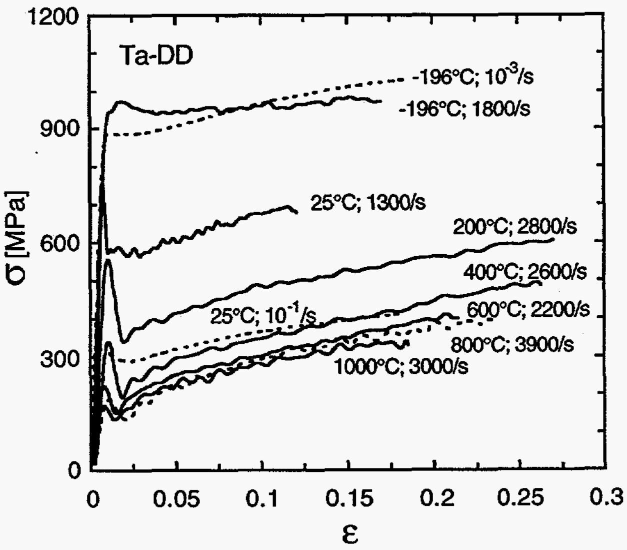

Figure 1: Compressive stress-strain response of an un-alloyed tantalum plate material.

A few common attributes are seen to be exhibited by these five sets of experimental data: 1) below 600°C at high strain rates, the yield stress is very sensitive to the testing temperature and strain rate, 2) most of the curves show stress drops immediately after yielding, the magnitude of this stress decrease depends strongly on the strain rate, and 3) all the materials hardened after yielding; however the rate of change in the flow stress at a certain strain is insensitive to both temperature and strain rate for tests below ≈400°C at high rates. Observations 1 and 3 are unique to materials with a body-centered-cubic structure. This behavior is primarily due to a strong Peierls barrier which is an intrinsic property of bcc metals and lower symmetry materials. Through thermal activation processes, this intrinsic barrier becomes transparent to dislocation motion at higher temperatures. The dependence of the flow stress on temperature therefore dramatically decreases (dynamic tests at 800 and 1000°C in Figure 1). On the contrary, for an annealed face-centered-cubic material (e.g., OFE-Cu or Ni-270) the yield stress weakly depends on the temperature and strain rate. In addition, the stress-strain curves at different temperatures and strain rates diverge upon further deformation indicating that their strain hardening behavior is rate dependent[30-32].

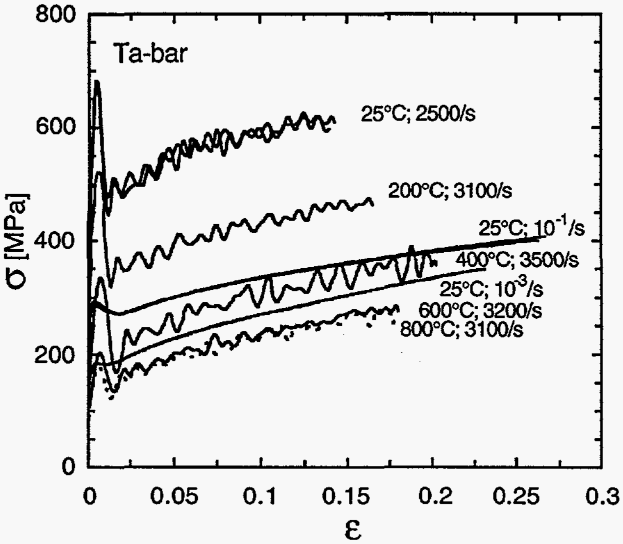

Figure 2: Compressive stress-strain response of the unalloyed tantalum bar material.

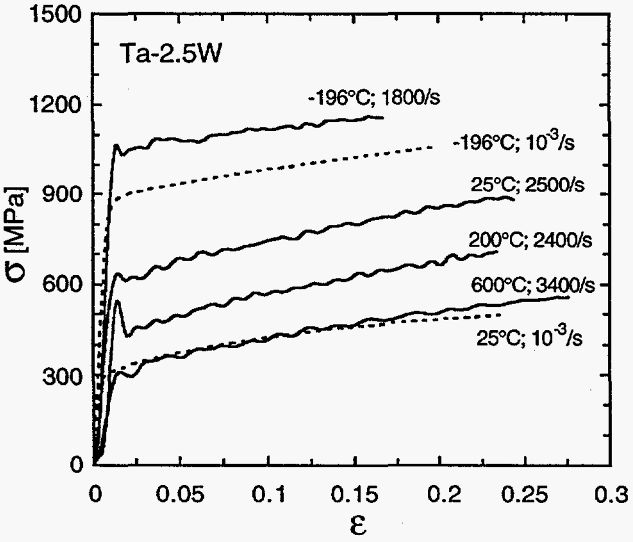

Figure 3: Compressive stress-strain response of the Ta-2.5W plate material.

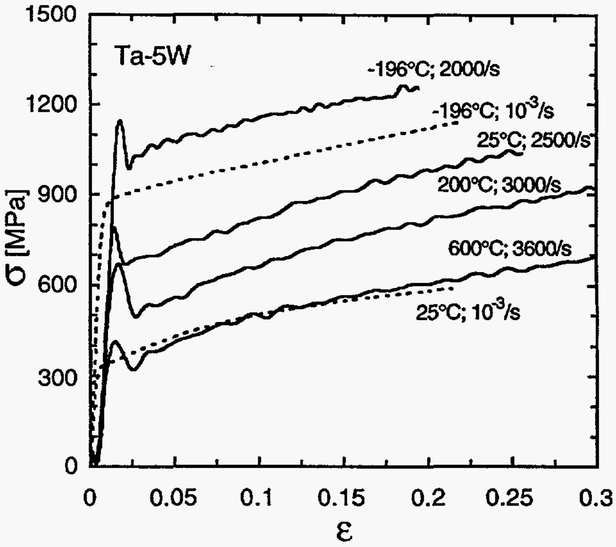

Figure 4: Compressive stress-strain response of the Ta-5W plate material.

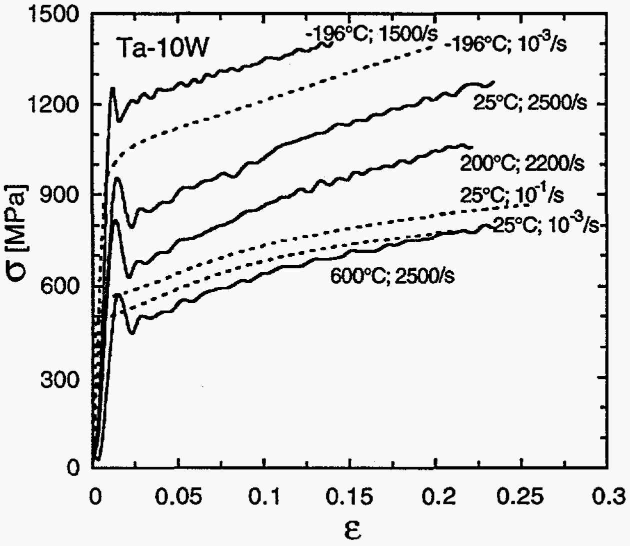

Figure 5: Compressive stress-strain response of the Ta-10W plate material.

The addition of tungsten to tantalum results in an increase in the yield stress and flow stresses at large strains in a similar way to increasing the strain rate for unalloyed tantalum. The room temperature stress-strain response of unalloyed tantalum at a strain rate of 2500 s^{-1} is very close to that exhibited by Ta-10W deformed at a strain rate of 10^{-3} s^{-1} at 25°C (Figure 6). This observation is consistent with well established solute strengthening effects of tungsten alloying additions on Ta[2,3]. The strain-rate and alloying effects on the flow stress response of Ta are quantified further in Figure 7 where the stress level at high, designated (hr), and low strain rates, designated (Lr), for two different strain values are plotted versus the tungsten alloying content in wt%. The stress levels at low strain rate are seen to increase linearly with alloying content (dashed lines with open symbols in Figure 7). At two different strain values (0.1 and 0.18), the linearity between the flow stresses and tungsten content is preserved with the same functional relationship suggesting that tungsten alloying doesn't alter the strain hardening behavior of these materials compressed at low strain rates at 25°C. The flow stresses obtained at the same strain under dynamic deformation (solid lines with solid symbols in Figure 7) increase more rapidly with respect to the alloying content compared to that exhibited under quasi-static conditions. The difference in the stress levels at high strain rate for strains of 0.1 and 0.18 increases with increasing alloying content. This divergence reveals the increase in strain hardening rate commensurate with increasing tungsten content in tantalum alloys. The flow stress differences between high- and low-strain-rate compression, given in Figure 7 as the finely dotted lines, increase with increasing tungsten content, except for the unalloyed tantalum which exhibits a higher difference than due to alloying with 2.5% tungsten. This discrepancy can be explained in terms of the high sensitivity of the flow stress to impurities in bcc materials at low temperature or high strain rate. Alloying with an ample quantity of tungsten tends to overshadow the impurity effects observed in lower purity tantalum. The flow stress drop after yielding (Figures 1-2), which was interpreted as an influence of impurities, during quasi-static deformation disappears when tantalum is alloyed with tungsten as shown in Figures 3-5. The flatness of the slope of the curves in Figure 7 describing the stress differences further indicates that the major influence of tungsten alloying on the mechanical properties of tantalum is to: 1) substantially raise the yield and flow stresses of tantalum with tungsten alloying, and 2) either weakly, as in the case of the 2.5 or 5 wt% alloys, or moderately, as in the 10 wt% alloy case, affect the strain-hardening response of tantalum.

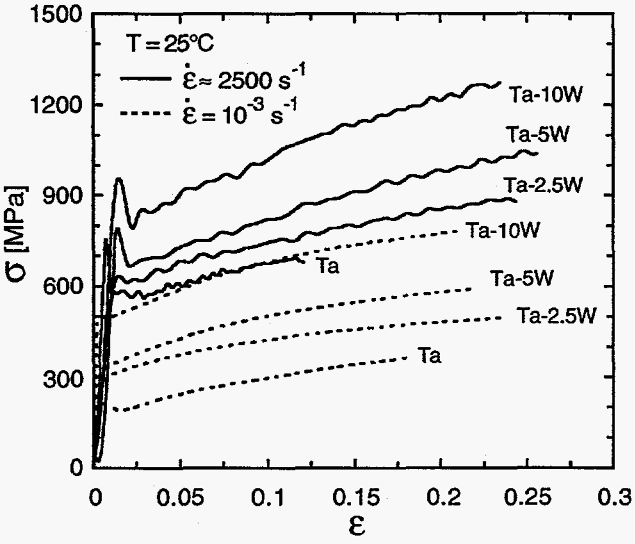

Figure 6: Compressive stress-strain response of the Ta and Ta-W plates.

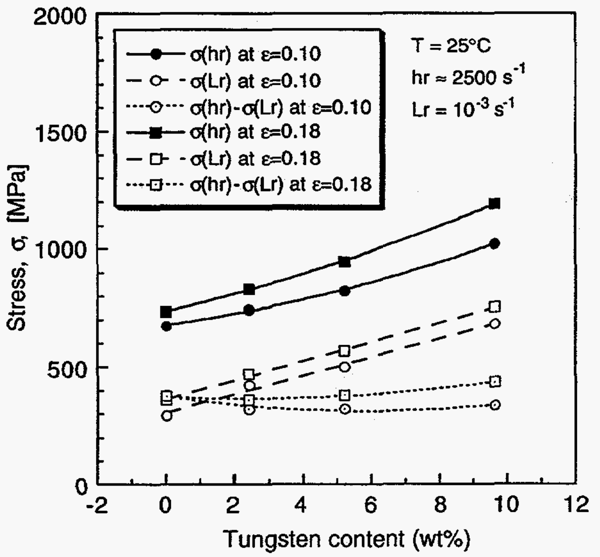

Figure 7: Room-temperature flow stresses at strains of 0.1 and 0.18 at strain rates of 2500 s^{-1} and 10^{-3} s^{-1} as a function of tungsten alloying content in tantalum.

The effect of temperature on alloyed tantalum can be realized through a similar plot as Figure 7 for four different materials dynamically deformed at 200 and at 600°C. For alloyed tantalum at 600°C (curves in Figures 3-5), the strain hardening behavior at strains greater than 0.1 starts to differ from the low-temperature behavior.

Alternate powder metallurgy processing routes were adopted to explore producing Ta materials exhibiting improved mechanical property reproducibility and isotropy as a focused goal for comparison with conventionally processed wrought Ta-plate or Ta-bar. The mechanical properties of these P/M materials were characterized in both compression and tension. The mechanical property test results provide information for guiding the LANL processing program toward the goal of producing high-density materials with specifically tailored or optimized properties.

The mechanical properties of several different P/M produced Ta materials were measured. Eight different P/M Ta materials were tested and a portion of the results of these studies are presented in Figures 8-10. Hot isostatically pressed (HIP'ed) Ta materials, starting with a high and low oxygen content, were tested over the same strain rate / temperature matrix used previously and are shown in Figures 8 and 9, respectively. The general features of the stress-strain behavior (rate sensitive flow stresses and rate insensitive strain hardening) observed previously in wrought Ta are preserved in these P/M materials. The high oxygen content P/M Ta exhibits a higher flow stress than either the lower oxygen P/M Ta or the wrought Ta plate, which exemplifies the effect of interstitial content on the mechanical properties of bcc materials. The flow stress of the high oxygen P/M Ta is about twice that of the Ta plate (Figures 1 and 8). The final composition of P/M Ta may change from the starting powders during processing. Analysis to determine the interstitial contents accurately is difficult to perform for bcc materials especially for Ta with an extremely high melting temperature. The chemical compositions listed in Table I should be used cautiously to derive any comparisons between the different Ta-materials based solely on the impurity contents.

Excellent reproducibility was demonstrated through repetitive processing from the same starting powders. Figure 10 shows quasi-static stress-strain curves at room temperature for four batches of P/M Ta. The Ta48A1 material was HIP'ed at 1600°C at 30 ksi for 2 hrs. The HIP'ing temperature for Ta48A2 was raised to 1800°C. The HIP'ing temperature, while changing the grain size, was found to have no detectable effect on the flow stress or strain hardening response. Ta48A3 and Ta48A4 were processed under the same conditions as Ta48A1. The HIP'ed Ta exhibited excellent consistency in its mechanical properties.

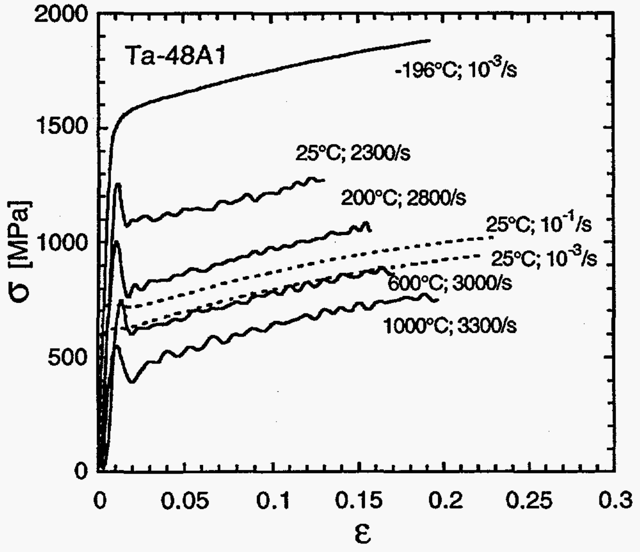

Figure 8: Compressive stress-strain response of a high oxygen content P/M Ta.

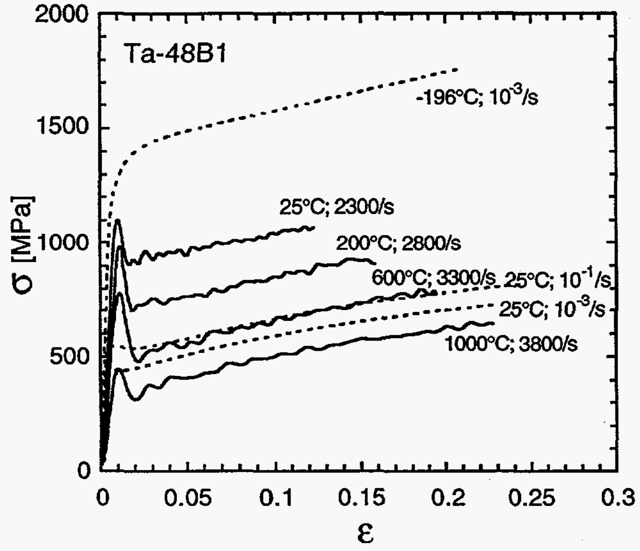

Figure 9: Compressive stress-strain response of a low oxygen content P/M Ta.

Constitutive Modeling of Ta-bar

Johnson-Cook and Zerilli-Armstrong Models:

The best fit to the ZA model for the Ta-bar material is shown in Figure 11. The experimental data at strains less than 0.2 were treated as representing an isothermal condition for all strain rates. The effect of adiabatic heating at high strain rates was neglected for low strains. The fitting results for the Ta bar to the ZA model are in close agreement with the experimental data for strain rates from 10^{-3} s^{-1} to 3200 s^{-1}, and temperatures ranging from 25°C to 600°C. For some applications, however, the stress levels at large strains are critically important. For this reason, after the best fit was derived from the low-strain data, the hardening exponent n was fixed to derive other sets of parameters for the ZA model. The formulation of the JC model (equation (1)) which was originally derived for fcc metals, presumes the stress-strain curves diverge upon deformation as is typical for metals such as Cu and Ni. The strain hardening rate is however insensitive to the strain rate and temperature change in unalloyed bcc materials like Ta within the range investigated. Substantial deviation from the experimental data for the JC model is therefore seen. The difference between the fitted value and the experimental data is expected to be larger at higher strains due to this divergence of the model. The fitting parameters for the Ta bar studied are listed in Tables II and III for the ZA model and the JC model, respectively.

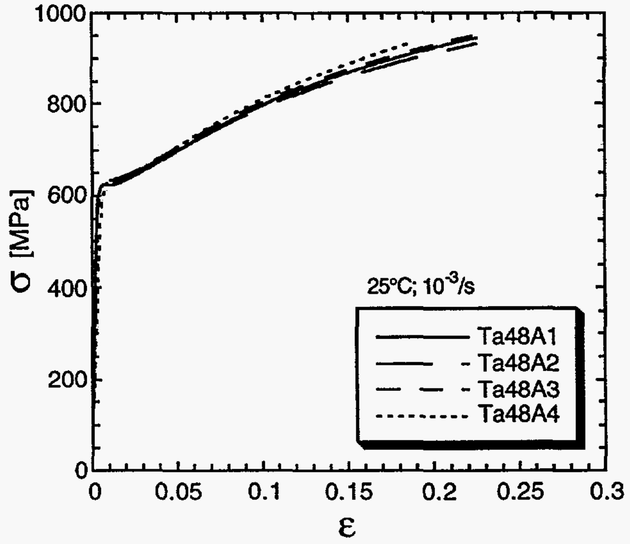

Figure 10: Compressive stress-strain response of four different high oxygen content (starting powders) P/M Ta.

Mechanical Threshold Model:

As stated in equation (5), the contributions to the flow stress from different obstacles needs to be examined to allow accurate physically-based materials modeling. The athermal stress depends on the temperature through the shear modulus only and it is a constant after being normalized by the shear modulus. Based on the data at low strain rates and high temperatures, a value of σ_a =40 MPa for Ta was chosen. The second term on the right hand side of equation (5) represents the thermal contribution to the yield stress on top of the athermal contribution. It is further assumed that this term does not evolve with strain. In well-annealed materials, the initial dislocation density is low so the contribution from the strain hardening term at very low strains can be neglected. From the plot of the yield stress (σ_y) as a function of the normalized activation energy, the corresponding parameters which describe the deviation from the mechanical threshold ($\hat{\sigma}_i$) as a function of temperature and strain rate can be determined. The governing equations (4) and (5) can be rearranged as

$$\left(\frac{\sigma_y-\sigma_a}{\mu}\right)^{p_i} = \left(\frac{\hat{\sigma}_i}{\mu_0}\right)^{p_i} - \left(\frac{kT}{g_{0i}\mu b^3}\ln\frac{\dot{\varepsilon}_{0i}}{\dot{\varepsilon}}\right)^{1/q_i} \cdot \left(\frac{\hat{\sigma}_i}{\mu_0}\right)^{p_i} \quad (12)$$

where $\dot{\varepsilon}_{0i}$ is an adjustable parameter. An optimum value will collapse all the data at different temperatures and strain rates into a single curve. g_{0i} is the activation energy for this process in units of μb^3. It is also an indication of the sensitivity of overcoming this obstacle to the change in temperature and strain rate. p_i and q_i are parameters with the range $0<p_i\leq 1$ and $1\leq q_i\leq 2$. They detail the glide resistance profile in the higher and lower activation energy regions, respectively[11]. Within the low normalized activation energy region (low temperature, higher strain rate), g_{oi} is relatively small ($\approx$0.13). The small value of the normalized activation energy suggests that the rate controlling mechanism in this material is overcoming the Peierls barrier which has a small activation volume[9,33].

The next step toward a complete constitutive relation for the MTS model is the description of the strain hardening due to dislocation storage. Constants used in equations (4)-(7) have to be determined from the experimental data. For each $\sigma(\varepsilon)$ curve, a corresponding mechanical threshold $\hat{\sigma}(\varepsilon)$ is derived according to equations (4) and (5). The hardening curve at 0K was fitted to equation (6) to obtain the saturation stress of the mechanical threshold. These saturation stresses at 0K were calculated for each test condition and the results were plotted according to equation (7) to derive the remaining parameters. Final model fitting results for the Ta bar are shown in Figure 13. The constants of the MTS model for the Ta bar are summarized in Table IV.

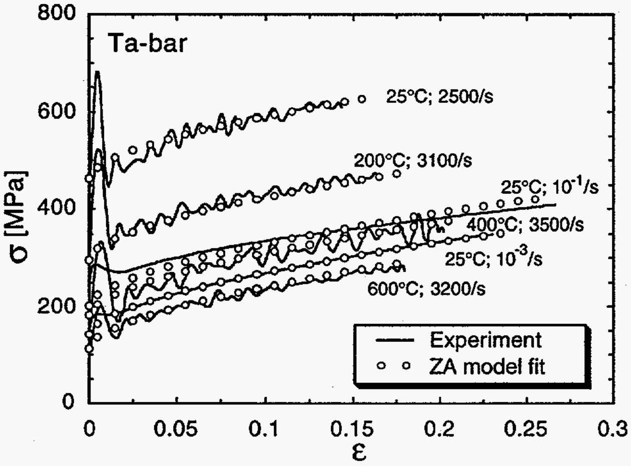

Figure 11: Zerilli-Armstrong model fit (symbols) for the annealed Ta bar material.

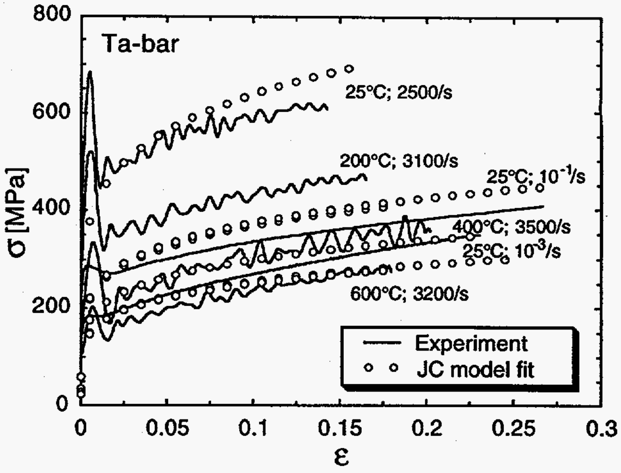

Figure 12: Johnson-Cook model fit (symbols) for the annealed Ta bar material.

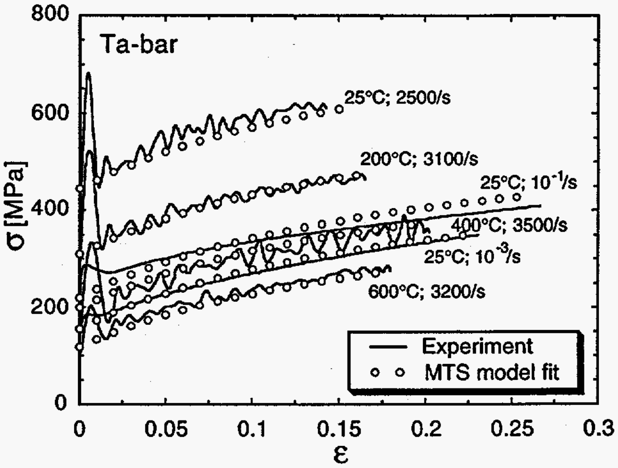

Figure 13: Mechanical Threshold Stress model fit (symbols) for the annealed Ta bar material.

The large-strain behavior of Ta is of particular relevance to some defense applications where the materials are subjected to dynamic deformation to large strains (e.g., explosive-formed penetrators, shape-charges, and Taylor impact tests). For the ZA and JC models, the strain hardening coefficient n depends on the range of strain over which the coefficient was optimized[34]. The best fit to small-strain data is achieved using n=0.575 for the ZA model (Figure 11). Fixed n-values of 0.5, 0.4 and 0.3 were then used to re-fit the data high-strain applications before the large-strain experimental data was available. The MTS model coefficients were derived based on the same well controlled low-strain data.

In this study various plastic strains (0, 0.42, 0.95 and 1.85) in Ta were achieved through upset forging cylinders of Ta-bar at room temperature. Compression samples were subsequently machined from the forged plates to study the mechanical properties associated with that degree of pre-straining. The thin surface layers, where surface shears due to friction during forging are known to dominate, were machined off the forged plates before the samples were cored from the plates using electro-discharge machining.

One needs to keep in mind the effect of deformation history effects on extrapolating large strain behavior to other loading paths. Tantalum is known to exhibit little or no dependence on deformation path[35] when deformation is dislocation-generation and storage dominated. Accordingly, the mechanical property data gathered through reloading the large-strain prestrained plates in this study can therefore be used to "check" the fit of constitutive models to large strains and thereafter applied to other deformation paths.

Prestrained samples were tested in compression at room temperature at a strain rate of 10^{-3} s^{-1}. The reload stress-strain responses after offsetting for the corresponding amount of prestrain are shown as the solid lines in Figure 14. It is seen that the reproducibility in the stress-strain response is diminished after pre-straining. The non-homogeneities in this Ta-bar which are documented in another paper in this proceedings clearly identified the existence of banding in the microstructure and a texture gradient in this material. Because of the scatter shown in the stress-strain data, the absolute large-strain behavior is not readily available. Since the reloaded samples were machined from various parts of the upset forged discs, the data can be viewed providing bounds on the mechanical response at large strains. Comparison with the model calculations is shown as open symbols in the same figure. The best fit of the ZA model to the small strain data with n=0.575 leads to an unrealistic stress level at large strains. Lower n-values seem to substantially decrease the stress levels at large strains. For the ZA model, n=0.3 seems to capture the large-strain behavior even though it totally missed the yield and low-strain experimental data (maganified as the insert in this figure). For constitutive models that use power hardening law, it is difficult to derive an optimum hardening coefficient if large-strain data is not available as is often the case since it is not trivial to obtain. The MTS model, due to its assumption of approaching saturation in stress at large strains, is able to satisfactorily "*predict*" the large-strain behavior based solely upon low-strain data. The "saturation" stress used in the MTS model for this particular strain rate and temperature will be achieved when the true strain exceeds 7. This is in excess of the strain range observed in many dynamic loading applications. Therefore, the saturation concept is used as a *limiting behavior* for the mechanical response in the MTS model, rather than a *demanding phenomenon* in constructing the model. The dependence of the n-value on the strain range optimized for the ZA and JC models makes it difficult to derive a unique set of material parameters covering a broad strain range. Extrapolation of the JC and ZA models to large strains therefore needs to be done carefully.

Table II Fitting parameters for Zerilli-Armstrong Model

	C_0 MPa	C_1 MPa	C_3 K^{-1}	C_4 $K^{-1} \cdot s^{-1}$	C_5 MPa	n
Ta-bar	25	1040	0.00525	0.0003	480	0.575
Ta-bar-large ε	5	1200	0.00650	0.00035	390	0.30

Table III Fitting parameters for Johnson-Cook Model

	A MPa	B MPa	n	C	m	T_{Melt} K	T_{Room} K
Ta-bar	185	675	0.3	0.047	0.425	3250	298

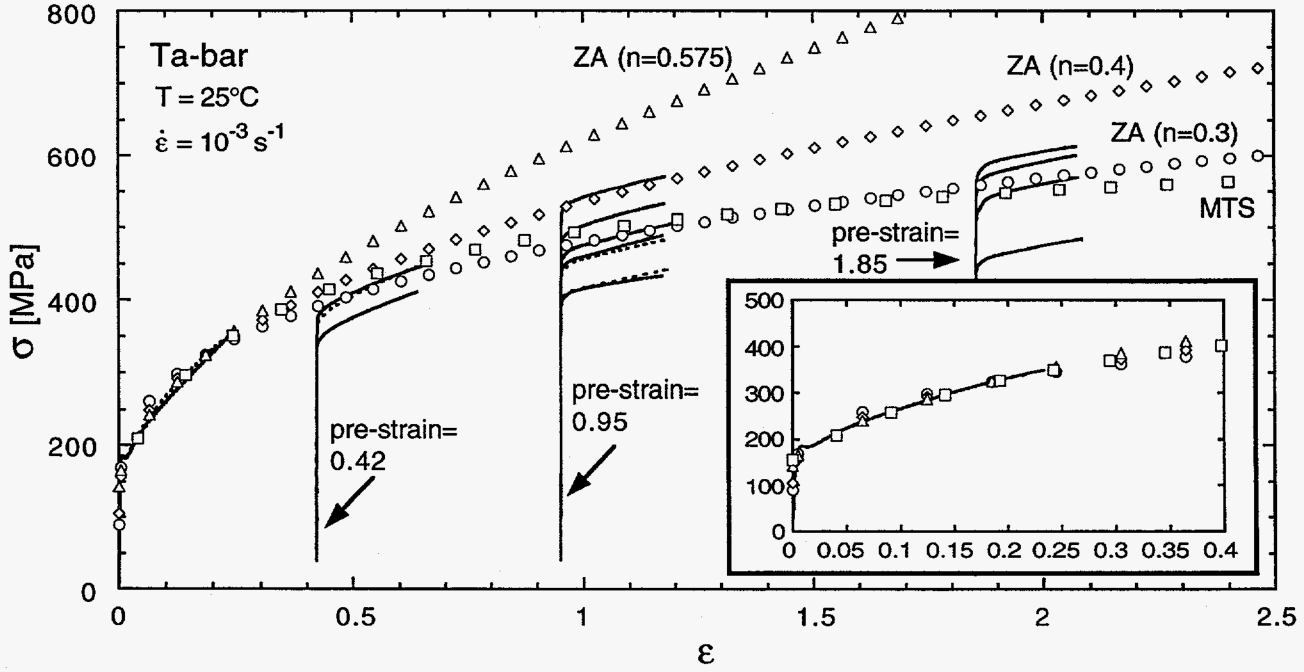

Figure 14: Compressive stress-strain response of the Ta-bar material as a function of upset forging strain.

Table IV Parameters for the MTS model

Equation	Parameter	Ta-bar	Units
(9)	μ_0	65250	MPa
μ	D	380	MPa
	T_0	40	K
(4), (7)	k/b^3	0.5881	MPa/K
	b	2.86×10^{-10}	m
(5)	σ_a	40	MPa
σ	$\hat{\sigma}_i/\mu_0$	0.014063	-
(4), (5)	g_{0i}	0.126852	-
S_i	$\dot{\varepsilon}_{0i}$	10^7	s^{-1}
	q_i	3/2	-
	p_i	1/2	-
(4), (5)	$\dot{\varepsilon}_{0\varepsilon}$	10^7	s^{-1}
S_ε	$g_{0\varepsilon}$	1.6	-
	q_ε	1	-
	p_ε	2/3	-
(6)	θ_0	2000	MPa
θ	α	2	-
(7)	$g_{0\varepsilon s}$	1.6	-
$\hat{\sigma}_{\varepsilon s}$	$\hat{\sigma}_{\varepsilon s0}$	470	MPa
	$\dot{\varepsilon}_{0\varepsilon s}$	10^7	s^{-1}
(10), (11)	ρ	16.6	Mg/m^3
ΔT	A_0	0.1455	$MPa\cdot m^3/Mg\cdot K$
	A_1 ($\times10^{-4}$)	0.09544	$MPa\cdot m^3/Mg\cdot K^2$
	A_2	-68.9	$MPa\cdot m^3\cdot K^3/Mg$
	Ψ	0.95	-

Deformation Mechanisms

The highly rate and temperature sensitivity of yielding behavior in bcc metals combined with almost rate-independent strain hardening has been the subject of numerous studies. The strong intrinsic barrier termed as Peierls stress is believed to be the major controlling mechanism. Long straight screw dislocations are readily evident in bcc metals deformed at low temperature. Because of the high Peierls stress, the material tends to create and propagate only those dislocations needed to respond to the external applied stresses. Dislocations with edge character travel faster than screws[36] leaving the screw dislocations behind. Gray and Vecchio recently[35] reported seeing, in the same materials used in this study that were deformed at room temperature to as much as 12% in strain, two sets of long straight screw dislocations as one of the main features in the substructure. Little interaction between these dislocations is observed implying that dynamic recovery has not been a dominant aspect in the deformation process. It has been reported that the activation volume of bcc metals doesn't vary systematically with strain further indicating that the density of obstacles remains essentially unchanged during deformation. Figure 15 shows such a probe by doing strain rate change tests. Continuous deformation at a constant strain rate is also plotted in this figure. The stress drop after yield is believed to be caused by dislocations unpinning from interstitials which is one type of a loading transient[37]. After passing this transient, the strain hardening behavior essentially is the same for the different strain rates. One of the strain rate jump tests was performed from a strain rate of 10^{-4} s^{-1} to 10^{-3} s^{-1} at strains of 0.05, 0.15, 0.25, and 0.35. The material was deformed at a high strain rate for a 3% interval in strain and then the strain rate was suddenly changed back to the lower one. The activation area and hence the strain rate sensitivity is determined from the increment in stress at the point of such a strain-rate jump. It is seen that the increment in stress is not a function of strain. The interesting observation is that the flow stress at higher strain rate reaches the same level as the flow stress of the material deformed solely at the higher strain rate. Another test with just one strain rate jump was performed at a strain of 0.2 from 10^{-4} s^{-1} to 10^{-2} s^{-1}. The flow stress immediately follows the continuous curve obtained at 10^{-2} s^{-1}. This data supports the supposition that the current structure at a given strain seems to be independent of the previous straining history.

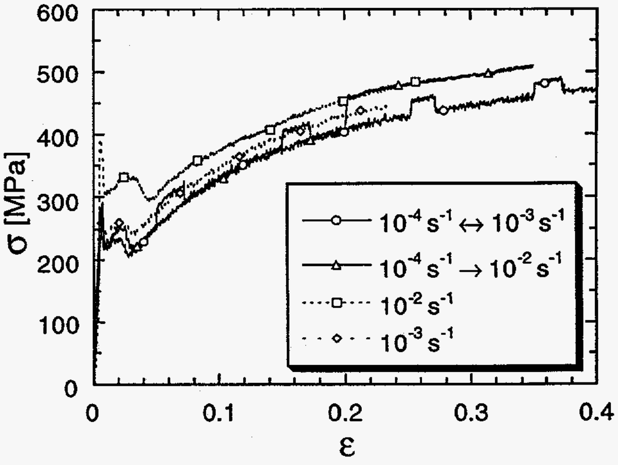

Figure 15: Compressive stress-strain response under continuous deformation condition and strain-rate jumps of the un-alloyed Ta-A plate material.

Initial portions (having more than 100 data points) of the stress-strain curves for five materials deformed at quasi-static strain rates at room temperature are summarized in Figure 16. For each material the strain hardening is essentially identical under these strain rates spanning 8% in strain. The slope of the curve for different materials is changed reflecting the solid solution hardening due to alloying. However, the individual set of stress-strain curves at two different strain rates for each material is almost parallel. A least-squares fit was fitted to a simple power-law equation $\sigma = \sigma_0 + k \cdot \varepsilon^n$ for the lower strain rate data to determine the hardening coefficient for each material. These coefficients are listed in Table V. The average n is 0.484. An n=1/2 works well if all dislocations are evenly distributed in the crystal such that the strain is related to the average effective distance that a dislocation travels before it is stopped.[38,39]:

$$\varepsilon \propto \rho b l, \tag{13}$$

ρ is the dislocation density. In this approach all dislocations are distributed uniformly, the average travel distance for a dislocation is then equal to the average distance between dislocations. The stress is traditionally written in terms of the dislocation density as[40]:

$$\sigma = \alpha \mu b \sqrt{\rho}, \tag{14}$$

where α is a geometrical constant with a typical value of 1/2. Combining the above two equations yields a parabolic relationship between stress and strain. From the result shown in Figures 15-17, it is suggested that the controlling deformation mechanism for Ta and Ta-W alloys is overcoming the Peierls stress. The high intrinsic Peierls stress inhibits cross slip of the screw dislocations and little or no dislocation annihilation occurs under this deformation condition. In addition to the Peierls stress, the strength of the obstacle either from impurities or other sets of screw dislocations is high enough to serve as an effective barrier to block the moving dislocations. The reduced effective glide distance for a dislocation results in increasing of dislocation density in order to respond to the external straining. The strain hardening at low strains is then related to the increase in dislocation density. Dislocations intersecting with forest dislocations resulting in strain hardening as well as softening (dynamic recovery mainly due to cross slip of screw dislocations) has not occurred to large extent at low strains as opposed to the typical response of fcc metals. The dislocation arrangements at a given effective strain are similar at the same deformation temperature[35] such that changing the strain rate suddenly forces the dislocations to travel at a faster speed and with less thermal activation available thereby results in an increase in the applied stress. At higher strains, the stress reaches a level high enough to force the dislocations to cut through the forest dislocations or surmount the impurities. Dislocation-dislocation interactions promote substructure rearrangements resulting in cell substructures forming at large strains[41]. A lower hardening coefficient n therefore is required if a power law is used as in the case shown in Figure 14.

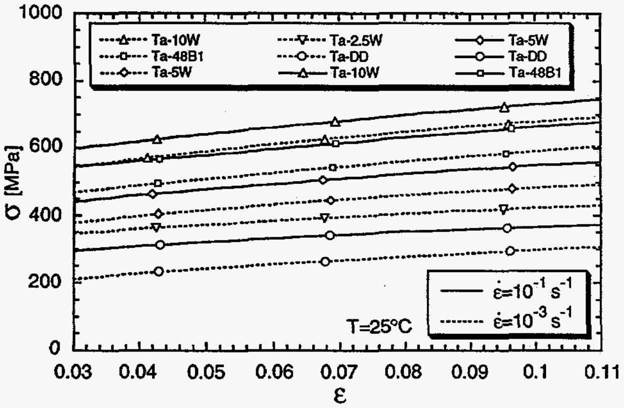

Figure 16: Compressive stress-strain response of the Ta-based materials.

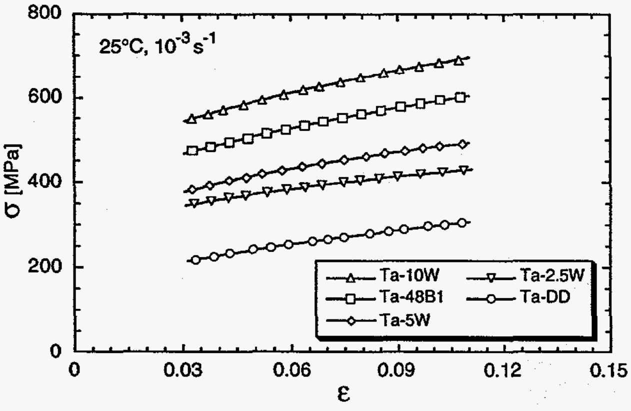

Figure 17: Best fit (lines) to the low-strain data (open symbols - only a fraction of the experimental data) for Ta and Ta-W using a simple power law between stress and strain.

Table V Best fitting coefficients to a power hardening law.

	σ_0, MPa	k, MPa	n
Ta-10W	373.5	962.6	0.495
Ta-48B1	344.0	952.4	0.585
Ta-5W	201.9	694.8	0.392
Ta-2.5W	210.3	511.0	0.382
Ta-DD	125.0	633.5	0.564

The deformation mechanism that controls the rate and temperature sensitivity of pure Ta and Ta with a small amount of alloying is a competing process between the intrinsic barrier due to a large Peierls stress, and the obstacles due to dislocation-dislocation interactions. At low temperatures or high strain rates, the Peierls stress dominates dislocation generation and propagation. Straight screw dislocations is one of the characteristics in the deformed structure. At higher strains, the stress increases high enough and the average dislocation distance decreases such that dislocation-dislocation interactions become significant. The strain hardening rate is a function of temperature and strain rate due to the process of dynamic recovery. Increasing the deformation temperature has a strong effect on the intrinsic barrier due to its small activation volume. The yield stress is no longer a strong function of temperature and strain rate. The generation and propagation of dislocations as well as cross slip becomes easy, the material exhibits deformation behavior very similar to that typical for fcc metals (Figure 18).

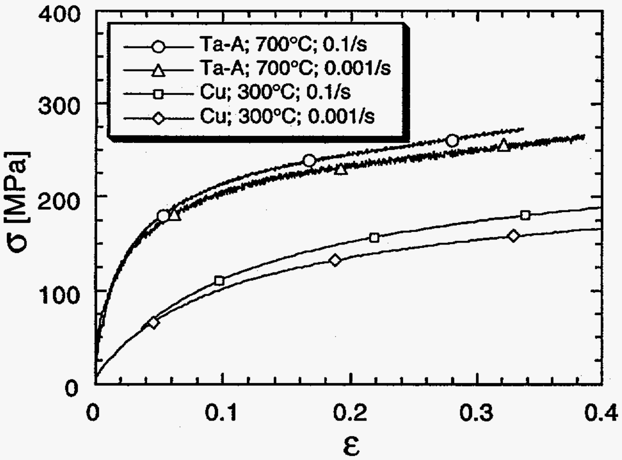

Figure 18: Compressive stress-strain curves for Ta-A and OFE-Cu[30] deformed at 700°C and 300°C respectively at low strain rates.

Summary

The current study of the mechanical properties and constitutive relations for tantalum and tantalum alloys under high strain-rate deformation yields the following observations:

(1). Tungsten alloying additions significantly increase the yield and flow stress levels attained and also increase the rate of work-hardening compared to unalloyed tantalum, under both quasi-static and dynamic strain rates.

(2). Three constitutive relations, namely the Johnson-Cook (JC), the Zerilli-Armstrong (ZA), and the Mechanical Threshold Stress (MTS) models, have been examined to describe stress-strain rate-temperature relations of Ta-bar in the high strain rate regime. The empirical relations used in the JC and ZA models for strain hardening $(\sigma_0 + K \cdot \varepsilon^n)$ may introduce substantial deviations from the actual stress levels at large strains if the coefficients were derived from the low-strain data. The physically-based MTS model overall provides better fitting results to cover the wider range of strains.

(3). The high strain-rate and temperature sensitivity of the flow stress and the insensitivity of the strain hardening rate indicate that the rate controlling mechanism for deformation at high strain rate from low to intermediate temperature in Ta and Ta-W alloys is thermal activation over the high Peierls stress. Dislocation-dislocation interactions become important at higher strains or at higher deformation temperatures. The operation of these two mechanisms changes the temperature and strain rate sensitivities of the yield stress and strain hardening behavior

Acknowledgements

The authors acknowledge the assistance of M.F. Lopez, R.W. Carpenter II for conducting the mechanical tests. The authors also acknowledge the effort in processing the Ta via powder metallurgy by V. Vargas, B. Roybal and P. Mombourquette. R. Trujillo and S. Atencio are acknowledged for conducting the upset forgings. This study was carried out under the auspices of the U.S. Department of Energy.

References

1. W. Kock and P. Paschen: Tantalum- Processing, Properties and Applications, *J. Metals*, 1989, vol. 41, pp. 33-39.
2. R.J. Arsenault and A. Lawley: Work-Hardening Characteristics of Ta and Ta-base Alloys, *Work Hardening*, J.P. Hirth and J. Weertman, eds., Gordon and Breach, New York, 1968, pp. 283-309.
3. G.T. Gray, III and A.D. Rollett: The High-Strain-Rate and Spallation Response of Tantalum, Ta-10W, and T-111, *High Strain Rate Behavior of Refractory Metals and Alloys*, R. Asfhani, E. Chen, and A. Crowson, eds., TMS, Warrendale, PA, 1992, pp. 303-315.
4. J.B. Clark, R.K. Garrett, Jr., T.L. Jungling, and R.I. Asfahani: Influence of Initial Ingot Breakdown on the Microstructural and Textural Development of High-Purity Tantalum, *Metall. Trans. A*, 1991, vol. 22A, pp. 2959-2968.
5. J.B. Clark, R.K. Garrett, Jr., T.L. Jungling, and R.I. Asfahani: Influence of Transverse Rolling on the Microstructural and Texture Development in Pure Tantalum, *Metall. Trans. A*, 1992, vol. 23A, pp. 2183-2191.
6. A. Gilbert, D. Hull, W.S. Owen, and C.N. Reid: The Yield of Polycrystalline Tantalum, *J. Less-Common Metals*, 1962, vol. 4, pp. 399-408.
7. J.W. Christian: Some Surprising Features of the Plastic Deformation of Body-Centered Cubic Metals and Alloys, *Metall. Trans.*, 1983, vol. 14A, pp. 1237-1256.
8. W.H. Gourdin, D.H. Lassila, M.M. LeBlanc, and A.L. Shields: The Influence of Tungsten Alloying on the Mechanical Properties of Tantalum, *DYMAT 94*, Oxford, UK, 1994.
9. K.G. Hoge and A.K. Mukherjee: The Temperature and Strain Rate Dependence of the Flow Stress of Tantalum, *J. Mater. Sci.*, 1977, vol. 12, pp. 1666-1672.
10. R.A. Foxall and C.D. Statham: Dislocation Arrangements in Deformed Single Crystals of Niobium-Molybdenum Alloys and Niobium-9at.% Rhenium, *Acta Metall.*, 1970, vol. 18, pp. 1147-1158.
11. U.F. Kocks, A.S. Argon, and M.F. Ashby: *Thermodynamics and Kinetics of Slip*, Prog. Mater. Sci., Vol. 19, Pergamon Press, New York, 1975.
12. W.H. Gourdin and D.H. Lassila: Multiple Mechanisms in the Thermally Activated Plastic Flow of Tantalum, *1995 APS Topical Conference*, Seattle, WA, 1995.
13. P.J. Maudlin, R.F. Davidson, and R.J. Henninger: Implementation and Assessment of the Mechanical-Threshold-Stress Model Using the EPIC2 and PINON Computer Codes, Technical Report- LA-11895-MS, Los Alamos National Laboratory, 1990.
14. M.N. Raftenberg: Modeling RHA Plate Perforation by a Shaped Charge Jet, Technical Report- BRL-TR-3363, U.S. Army Ballistic Research Laboratory, 1992.
15. A.M. Rajendran and P. Woolsey: Penetration of Tungsten Alloy Rods Into Shallow-Cavity Steel Targets, Technical Report- ARL-TR-216, U.S. Army Research Laboratory, 1993.

16. P.S. Follansbee and U.F. Kocks: A Constitutive Description of Copper Based on the Use of the Mechanical Threshold Stress as an Internal State Variable, *Acta Metall.*, 1988, vol. 36, pp. 81-93.
17. G.R. Johnson and W.H. Cook: A Constitutive Model and Data for Metals Subjected to Large Strains, High Strain Rates and High Temperatures, *Proceedings of the Seventh International Symposium on Ballistic*, The Hague, The Netherlands, 1983, pp. 541-547.
18. F.J. Zerilli and R.W. Armstrong: Dislocation-mechanics-based Constitutive Relations for Material Dynamics Calculations, *J. Appl. Phys.*, 1987, vol. 61, pp. 1816-1825.
19. G.T. Gray, III, S.R. Bingert, S.I. Wright, and S.R. Chen: Influence of Tungsten Alloying Additions on the Mechanical Properties and Texture of Tantalum, *High Temperature Silicides and Refractory Alloys*, C.L. Briant, J.J. Petrovic, B.P. Bewlay, A.K. Vasudevan, and H.A. Lipsitt, eds., Proc. Vol. 322, Materials Research Society, Pittsburgh, PA, 1994, pp. 407-412.
20. P.S. Follansbee: *High Strain Rate Compression Testing - The Hopkinson Bar,* 9th edn. Vol. 8, Am. Soc. Metals, Metals Park, Ohio, 1985, pp. 198-203.
21. P.S. Follansbee and G.T. Gray, III: An Analysis of the Low Temperature and High-Strain-Rate Deformation of Ti-6Al-4V, *Metall. Trans. A*, 1989, vol. 20A, pp. 863-874.
22. P.S. Follansbee, J.C. Huang, and G.T. Gray, III: Low-Temperature and High-Strain-Rate Deformation of Nickel and Nickel-Carbon Alloys and Analysis of the Constitutive Behavior According to An Internal State Variable Model, *Acta Metall.*, 1990, vol. 38, pp. 1241-1254.
23. S.R. Chen and G.T. Gray, III: Constitutive Behavior of Tungsten and Tantalum: Experiments and Modeling, *2nd International Conference on Tungsten and Refractory Metals*, A. Bose and R.J. Dowding, eds., October 17-19, McLean, VA, Metal Powder Industries Federation, Princeton, New Jersey, 1995, pp. 489-498.
24. U.F. Kocks: Laws for Work-Hardening and Low-Temperature Creep, *J. Eng. Mater. Tech., Trans. ASME*, 1976, vol. 98, pp. 76-85.
25. P. Hassen: Plastic Deformation of Nickel Single Crystals at Low Temperatures, *Phil. Mag.*, 1958, vol. 3, pp. 384-418.
26. G. Schoeck and A. Seeger: *Defects in Crystalline Solids*, Physical Society, London, 1955.
27. G. Simmons and H. Wang: *Single Crystal Elastic Constants and Calculated Aggregate Properties: A Handbook*, 2nd edn., The M.I.T. Press, Boston, Mass., 1991.
28. Y.P. Varshni: Temperature Dependence of the Elastic Constants, *Phys. Rev. B*, 1970, vol. 2, pp. 3952-3958.
29. D.R. Stull and G.C. Sinke, eds.: *Thermodynamic Properties of the Elements*, American Chemical Society, Washington D. C., 1956.
30. S.R. Chen and U.F. Kocks: High-Temperature Plasticity in Copper Polycrystals, *High Temperature Constitutive Modeling - Theory and Application*, A.D. Freed and K.P. Walker, eds., Atlanta, GA, The American Society of Mechanical Engineers, 1991, pp. 1-12.
31. U.F. Kocks and S.R. Chen: On the Two Distinct Effects of Thermal Activation on Plasticity: Application to Nickel, *phys. stat. sol. (a)*, 1992, vol. 131, pp. 403-413.
32. U.F. Kocks, S.R. Chen, and H. Mecking: Is There a Unique Effective Interaction Profile for Dislocations, *Advances in Crystal Plasticity*, D.S. Wilkinson and J.D. Embury, eds., Kingston, Ontario, Canada, Canadian Institute of Mining, Metallurgy and Petroleum, 1992, pp. 87-112.
33. H. Conrad: Thermally Activated Deformation of Metals, *J. Metals*, 1964, vol. 16, pp. 582-588.
34. G.T. Gray, III, S.R. Chen, and K.S. Vecchio: Influence of Grain Size on the Constitutive Response and Substructure Evolution of MONEL 400, *to be submitted*, 1996.
35. G.T. Gray, III and K.S. Vecchio: Influence of Peak Pressure and Temperature on the Structure/Property Response of Shock-Loaded Ta and Ta-10W, *Metall. Trans. A*, 1995, vol. 26A, pp. 2555-2562.
36. W.G. Johnston and J.J. Gilman: Dislocation Velocities, Dislocation Densities, and Plastic Flow in Lithium Fluoride Crystals, *J. Appl. Phys.*, 1959, vol. 30, pp. 129-144.
37. U.F. Kocks: *Constitutive Behavior Based on Crystal Plasticity*, Elsevier, 1987, pp. 1-88.
38. G.I. Taylor: The Mechanism of Plastic Deformation of Crystals. Part I. - Theoretical, *Pro. Roy. Soc.*, 1934, vol. A145, pp. 362-387.
39. G.I. Taylor: The Mechanism of Plastic Deformation of Crystals. Part II. - Comparison with Observations, *Pro. Roy. Soc.*, 1934, vol. A134, pp. 388-404.
40. H. Wiedersich: Hardening Mechanisms and the Theory of Deformation, *J. Metals*, 1964, vol. 16, pp. 425-430.
41. D.A. Hughes: Deformation Microstructures in Refractory Metals and Alloys: Past and Present Research, *Evolution in Refractory Alloys Symposium*, E.N.C. Dalder, T. Grobstein, and C.S. Olsen, eds., Denver, TMS, 1993, pp. 219-235.

DISCLAIMER

This report was prepared as an account of work sponsored by an agency of the United States Government. Neither the United States Government nor any agency thereof, nor any of their employees, makes any warranty, express or implied, or assumes any legal liability or responsibility for the accuracy, completeness, or usefulness of any information, apparatus, product, or process disclosed, or represents that its use would not infringe privately owned rights. Reference herein to any specific commercial product, process, or service by trade name, trademark, manufacturer, or otherwise does not necessarily constitute or imply its endorsement, recommendation, or favoring by the United States Government or any agency thereof. The views and opinions of authors expressed herein do not necessarily state or reflect those of the United States Government or any agency thereof.